ACS APPLIED MATERIALS & INTERFACES

Research Article

www.acsami.org

pH-Responsive Shape Memory Poly(ethylene glycol)−Poly(ε-caprolactone)-based Polyurethane/Cellulose Nanocrystals Nanocomposite

Ying Li, Hongmei Chen, Dian Liu, Wenxi Wang, Ye Liu, and Shaobing Zhou*

Key Laboratory of Advanced Technologies of Materials, Ministry of Education, School of Materials Science and Engineering, Southwest Jiaotong University, Chengdu, Sichuan 610031, People's Republic of China

Supporting Information

ABSTRACT: In this study, we developed a pH-responsive shape-memory polymer nanocomposite by blending poly(ethylene glycol)−poly(ε-caprolactone)-based polyurethane (PECU) with functionalized cellulose nanocrystals (CNCs). CNCs were functionalized with pyridine moieties (CNC−$C_6H_4NO_2$) through hydroxyl substitution of CNCs with pyridine-4-carbonyl chloride and with carboxyl groups (CNC−CO_2H) via 2,2,6,6-tetramethyl-1-piperidinyloxy (TEMPO) mediated surface oxidation, respectively. At a high pH value, the CNC−$C_6H_4NO_2$ had attractive interactions from the hydrogen bonding between pyridine groups and hydroxyl moieties; at a low pH value, the interactions reduced or disappeared due to the protonation of pyridine groups, which are a Lewis base. The CNC−CO_2H responded to pH variation in an opposite manner. The hydrogen bonding interactions of both CNC−$C_6H_4NO_2$ and CNC−CO_2H can be readily disassociated by altering pH values, endowing the pH-responsiveness of CNCs. When these functionalized CNCs were added in PECU polymer matrix to form nanocomposite network which was confirmed with rheological measurements, the mechanical properties of PECU were not only obviously improved but also the pH-responsiveness of CNCs could be transferred to the nanocomposite network. The pH-sensitive CNC percolation network in polymer matrix served as the switch units of shape-memory polymers (SMPs). Furthermore, the modified CNC percolation network and polymer molecular chains also had strong hydrogen bonding interactions among hydroxyl, carboxyl, pyridine moieties, and isocyanate groups, which could be formed or destroyed through changing pH value. The shape memory function of the nanocomposite network was only dependent on the pH variation of the environment. Therefore, this pH-responsive shape-memory nancomposite could be potentially developed into a new smart polymer material.

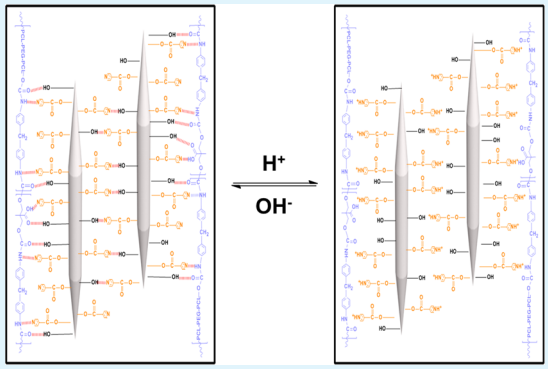

KEYWORDS: *shape memory, pH-responsive, percolating network, nanocomposite, cellulose nanocrystals*

INTRODUCTION

Shape-memory polymers (SMPs), as one of the most important branches of smart materials, are able to fix into a temporary shape and then recover to their original shape[1] when exposed to an environmental stimulus such as heat,[2−4] light,[5,6] electric field,[7−9] magnetic field,[10,11] solvent,[12−14] or redox.[15,16] SMPs have many potential applications in the design of therapeutic strategies,[17] such as aneurysm occlusion devices,[18] esophageal stent,[19] tissue engineering scaffold,[20] and drug delivery.[21,22] Despite the demonstrated merits, the low mechanical properties of the SMPs limit their applications. Incorporating stiff fillers or fibers is an effective way to increase the mechanical properties of SMPs,[23] such as SiO_2,[24] nanoclay,[25] carbon nanotubes,[26] Fe_3O_4 nanoparticles[27] and CNCs.[28] Among these fillers, CNCs have such advantages as high crystallinity, large surface area, excellent mechanical strength, and so on. CNCs also have many OH groups on their surfaces, which leads to strong hydrogen bonding interactions between CNCs and matrix materials.[28] Due to their superior physical and chemical properties, CNCs have received much attention in the field of nanocomposites.[29]

The shape memory effect (SME) of shape-memory polymer composites (SMPCs) is anticipated to be conveniently controlled with a mild stimulus. The SMPCs that incorporate CNCs in the polymer matrix display a innovative water-induced SME and change their mechanical properties upon exposure to water, which has been developed in recent years.[30−32] In these composites, the CNC percolation network in matrix materials serves as the switch units of SMPs, leading to an unprecedented rapidly switchable SME that may be activated by water. This is due to more hydrogen bonding interactions between CNC percolation network and matrix materials reversible formation

Received: April 5, 2015
Accepted: May 26, 2015
Published: May 26, 2015

DOI: 10.1021/acsami.5b02940
ACS Appl. Mater. Interfaces 2015, 7, 12988−12999

and destruction during the wetting and drying cycle.[33−35] This SMP is totally different from the traditional water-induced SMPs, which belong to indirect thermal-sensitive SMPs. The water as plasticizer reduces transition temperature of SMPs, and then the SMPs recover their original shape at room temperature.[36]

Different sites of the body have variations in physiological pH values. In particular pathological conditions, the physiological pH of biological systems generally appears a sharp gradient.[37] Compared with the thermal-sensitive SMPs and indirect thermal-sensitive such as light, electric, magnetic induced SMPs limited in biomedical applications, the pH-induced SMP is an ideal candidate for designing biomedical applications.[38] So far, there have been several reports about pH-sensitive SMPs. For example, Zhang et al. reported a pH-sensitive SMP prepared with β-cyclodextrin modified alginate and diethylenetriamine modified alginate.[39] Willner et al. reported pH-stimulated DNA hydrogels exhibiting shape-memory properties.[40] Our group previously developed a pH-sensitive SMP based on polyurethane.[38] However, in these systems, the pH-induced shape memory effect was realized by the polymer material itself via polymer swelling at different pH values. At the same time, the mechanical properties of these materials are poor. To address these problems, adding functionalized CNCs into polymer to form polymer composites is an effective strategy. Chen et al. reported biomimetic polymer composites by using chitosan-modified cellulose whiskers as the stimulus-responsive phase and thermoplastic polyurethane as the resilient matrix, which represented water-active mechanically adaptive and shape-memory behavior in different pH environments.[41]

In this study, we developed a pH-responsive SMP nanocomposite by blending poly(ethylene glycol)−poly(ε-caprolactone)-based polyurethane (PECU) with functionalized cellulose nanocrystals (CNCs). CNCs were functionalized with pyridine moieties (CNC−$C_6H_4NO_2$) through hydroxyl substitution of CNCs with pyridine-4-carbonyl chloride and with carboxyl groups (CNC−CO_2H) via TEMPO-mediated surface oxidation, respectively. At pH values below 5, the pyridine groups on the surface of CNC−$C_6H_4NO_2$ were protonated because the pyridine groups were a Lewis base. At pH values above 5, CNC−$C_6H_4NO_2$ had attractive hydrogen bonding interactions between hydroxyl moieties and pyridyl group.[38,42] The CNC−CO_2H could be expected to respond to pH variation in an opposite manner. At high pH, the CNC−CO_2H were ionized and negatively charged; therefore, the attractive interactions between the CNCs could be reduced by electrostatic repulsions. Conversely, at low pH, the CNC−CO_2H had attractive interactions, which resulted from hydrogen bonding of the carboxylic acid and hydroxyl moieties.[43] PECU was obtained by, first, the synthesis of PCL−PEG-PCL by the ring-opening polymerization of ε-caprolactone (ε-CL) with poly(ethylene glycol) (PEG) and, second, getting the resultant polymer with PCL−PEG-PCL as the soft segment of polyurethane (PU) matrix materials by the reaction of PCL−PEG-PCL with 4,4-diphenylmethane diisocyanate (MDI) in the presence of chain extender DMPA. The introduction of the PCL−PEG-PCL segment can enhance the biodegradation and biocompatibility of the resultant polymer. The matrix materials with good mechanical properties, which obtained through the physical composite modified CNCs. In this nanocomposite system, the pH-sensitive SME is realized through the association and dissociation of the hydrogen bond interactions between the modified CNCs percolation network and matrix materials (Figure 1 and Figure S1, Supporting Information).

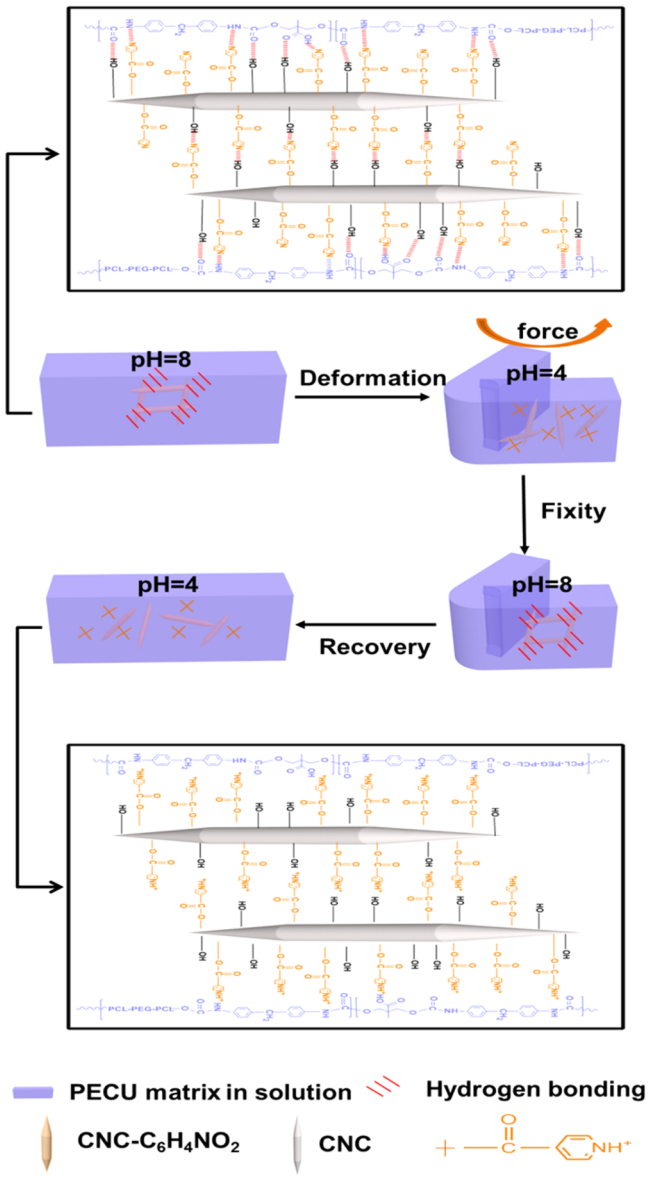

Figure 1. Schematic representation of the pH-responsive shape-memory materials, which rely on hydrogen bonding switching mechanism in the interactions between cellulose nanocrystals (CNC−$C_6H_4NO_2$) within polymer matrix upon immersion in HCl solution (pH = 4) or NaOH solution (pH = 8).

The pH-sensitive CNCs percolation network serves as the switch units of SMPs; both the PECU physical cross-linking and microphase separation act as the net-point.[44]

MATERIALS AND METHODS

Materials. Poly(ethylene glycol) (PEG, M_n 2.0 kDa) were recrystallized before use, *N*,*N*-dimethylformamide (DMF), 2,2,6,6-tetramethyl-1-piperidinyloxy (TEMPO), NaBr, NaOCl, isonicotinic acid, thionyl chloride ($SOCl_2$), triethylamine were reflux redistilled before used and stannous chloride ($SnCl_2$) were purchased from Kelong Chemical Reagent Factory in Chengdu. ε-Caprolactone (ε-CL), Stannous octoate [$Sn(Oct)_2$, 95%] were purchased from Aldrich. DMF was dried as our group previously report.[38] 4,4-Diphenylmethane diisocyanate (MDI), was purchased from Tokyo Chemical

DOI: 10.1021/acsami.5b02940
ACS Appl. Mater. Interfaces 2015, 7, 12988−12999

Scheme 1. (a) Synthetic Procedure of the Modified Cellulose Nanocrystals (1) CNC−$C_6H_4NO_2$ and (2) CNC−CO_2H and (b) Synthetic Route of PECU Polymer; (inset) Internal Structure of Cellulose Nanocrystals; Modification Occurs on the Surface of Cellulose Nanocrystals.

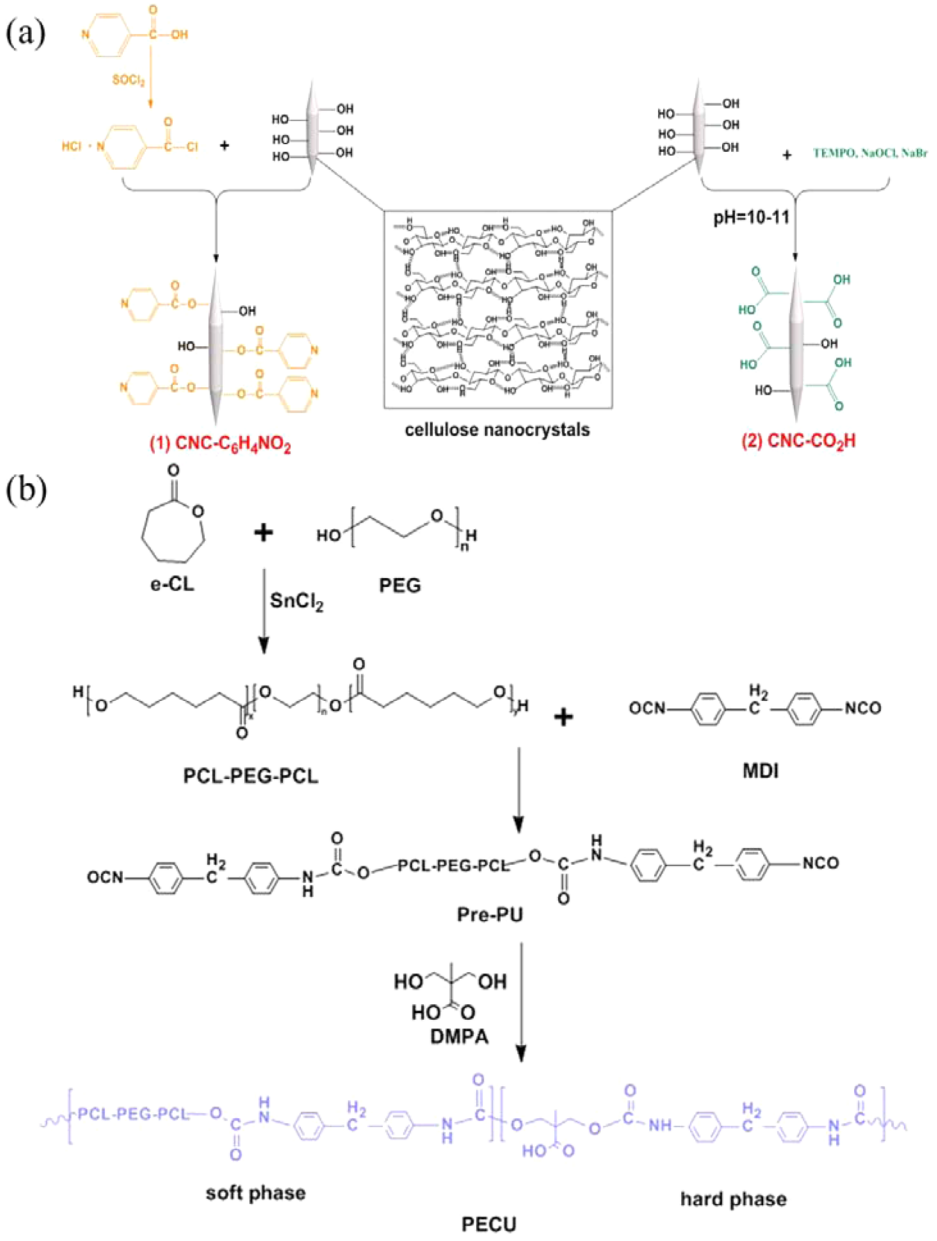

industry Co., Ltd. ε-CL was purified by drying over CaH_2 and distilled under reduced pressure. 2,2-Bis(hydroxymethyl) propionic acid (DMPA, 99%) was purchased from Acros Organics. CNCs were preparedaccording to the previous literature.[45]

Preparation of Pyridine Moieties Modified Cellulose Nanocrystals (CNC−$C_6H_4NO_2$). The CNCs stable suspension in DMF was achieved with a solid content of 20 mg/mL in our group's earlier work, in which the detailed experimental description has already been provided.[46] The amount (2.9 ± 0.2 mmol/g) of reactive hydroxyl group on cellulose nanocrystals was measured by titration of excessive isocyanate groups.[47] Pyridine-4-carbonyl chloride was synthesized by isonicotinic acid and $SOCl_2$ as described previously.[48] Pyridine-4-carbonyl chloride (2 g) and triethylamine (1 g) were added to a dried three-necked flask under stirring and Ar gas protection device. Later, ultrasonic treatment CNCs suspension in DMF (30 mL) was added dropwise into three-necked flask. The reaction was carried out at 80 °C for 24 h. The resultant suspension was subsequently distilled under reduced pressure and washed by continuous centrifugation with deionized water. Finally, CNC−$C_6H_4NO_2$ suspension in DMF was obtained by solvent-exchange sol−gel process, as described previously (Scheme 1a1).[46] From the nitrogen content according to eq 1, the degree of substitution (DS) of modified cellulose nanocrystals was calculated:

$$\mathrm{N\%} = \frac{\mathrm{DS} \times 14 \times M}{162 + \mathrm{DS} \times \mathrm{MWG}} \quad (1)$$

where N% the is weight percentage of nitrogen, M is number of nitrogen atoms in the substituent group, and MWG is the molecular weight of the substituent group.[49]

Preparation of Carboxylic Acid Modified Cellulose Nanocrystals (CNC−CO_2H). Ultrasonic treatment CNCs suspension in water (20 mg/mL, 30 mL) were added into a dried three-necked flask with magnetic stirring, which was connected to the backflow device and Ar gas protection device. TEMPO (0.02 g), NaBr (0.2 g), and NaOCl (1.76 M, 0.5 mL, 0.88 mmol) were stirred in 10 mL of water until completely dissolved. This solution was then added to the CNCs

DOI: 10.1021/acsami.5b02940
ACS Appl. Mater. Interfaces 2015, 7, 12988−12999

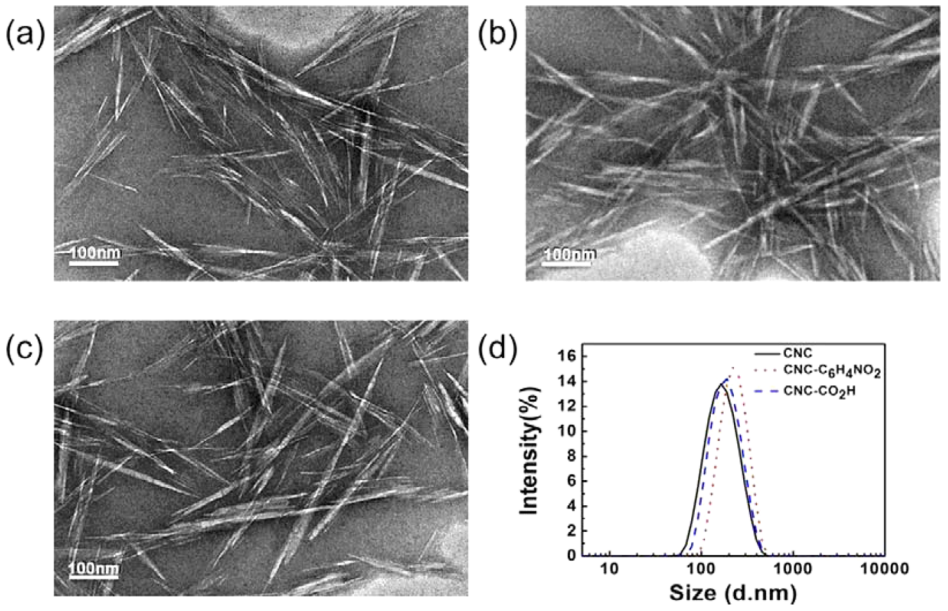

Figure 2. Transmission electron micrographs of (a) CNC, (b) CNC−$C_6H_4NO_2$, and (c) CNC−CO_2H. (d) Size analysis.

suspension.[52] The pH of the mixture was maintained at 10 by adding 0.5 M NaOH while the suspension was stirred at room temperature. After 5 h, methanol (ca. 2 mL) was added, terminating the oxidation, and the pH was adjusted to 7 with 0.5 M HCl. The water suspension of CNCs was recovered by centrifugation and washed with water. The oxidized CNCs were dialyzed and then CNC−CO_2H suspension in DMF was obtained by solvent-exchange sol−gel process as previously described (Scheme 1a2).[46] Conductimetric titration curves allow us to calculate the amount of carboxyl groups and the degree of oxidation (DO), which is given by eq 2:

$$\mathrm{DO} = \frac{162 \times C \times (\mathrm{V2} - \mathrm{V1})}{w - 36 \times C \times (\mathrm{V2} - \mathrm{V1})} \quad (2)$$

where C is the NaOH concentration (mol/L), V1 and V2 are the amount of NaOH (Supporting Information), w is the weight (g) of the oven-dried sample, the value of 36 corresponds to the difference between the molecular weight of an anhydroglucose unit (AGU) and that of the sodium salt of a glucuronic acid moiety.[50]

Preparation of PECU and its Nanocomposites. PCL−PEG-PCL(PCL/PEG molecular mass ratio, 6:4) was first synthesized by ring-opening polymerization method.[51] Number-average molecular weight (M_n) and polydispersity were measured by gel permeation chromatography (GPC). The detection method of GPC (Waters 1515) measurement was previously reported by our group.[38] PCL−PEG-PCL (0.36 mmol) were added into a three-necked round flask and dried at vacuum under a reduced pressure at 80 °C for 2 h. Then MDI (0.92 mmol) were added to this flask under stirring and Ar gas protection device. The reaction was carried out at 80 °C for 2 h to prepare the prepolymer. After that, MDI (1.54 mmol), $Sn(Oct)_2$ and chain extender DMPA (2.1 mmol) were added into the reaction system at 80 °C for another 2 h. The solution was poured out and evaporated at 80 °C for 8 h to obtain films. These films were further dried under vacuum at room temperature for another 48 h (Scheme 1b). The PECU called as $(PCL−PEG-PCL)_{70\%}$-MDI-DMPA, in which the numerical values under the PCL−PEG-PCL indicate the weight percent of PCL−PEG-PCL in the PECU (M_n 16.9 kDa, polydispersity 1.1 measured by the GPC system). The PECU was dissolved in DMF at a concentration of 50 mg/mL by stirring for 4 h. CNC−$C_6H_4NO_2$ or CNC−CO_2H suspension in DMF was prepared by ultrasonic treatment and subsequently added into PECU solutions according to the concentrations of 5, 10, 20, and 30 wt % (modified CNCs/PECU). The numerical values under the CNCs indicate the weight percent of CNCs in the nanocomposites. After these mixtures were stirred for 6 h, they were cast into Teflon dishes, and evaporated at 60 °C for 8 h to acquire films. The films were further dried under vacuum at room temperature for another 48 h and subsequently dried under vacuum at 80 °C for 12 h to remove residual solvent.

Characterization. ^{1}H NMR was performed on a Varian 400 NMR spectrometer. The detection method of Fourier transform infrared spectroscopy (FT-IR) of all CNCs samples were conducted as our group previously report.[48] Each nanocomposite sample was prepared by using a film, which was tested after immersion in HCl solution at pH = 1 or 4 and NaOH solution at pH = 8 or 10, respectively, for 60 min. The detection method of X-ray photoelectron spectroscopy (XPS) as our group previously reported.[46] Elemental analysis was carried out using Micro Analysis (Euro EA 3000) Elementar instrument (Table S1, Supporting Information). The carboxyl content of oxidized CNCs samples was determined by conductometric titration (Rex DDS-307A). The detailed experimental description has already been provided.[50]

The average size and zeta potential of CNCs were determined by dynamic light scattering (DLS; Zeta-Sizer, Malvern Nano-ZS90, Malvern, U.K.) at 25 °C. The morphologies of CNCs were tested by transmission electron microscopy (TEM) with JEOL 2100F instrument (JEOL Ltd., Japan) operated at 200 kV. The detection method of the fracture surfaces of the composites were investigated as our group previously reported.[46] The swelling degree of the samples was calculated by measuring the samples weight before and after immersed in HCl solution (pH = 1 or 4) or NaOH solution (pH = 8 or 10) at room temperature. The weight ratio of absorbed solution was calculated as our group previously reported.[46] Contact angle equipment (DSA 100, KRUSS) was investigated as our group previously reported.[46] The retained time of the water drop on the sample surface was 30 s.

Differential scanning calorimetry (DSC) measurements were performed as our group previously reported.[46] X-ray diffractometry (XRD) was investigated as our group previously report.[46] The tensile properties of the samples at room temperature were performed on an Instron 5567 (Instron Co., Massachusetts) instrument. The extension rate was 1 mm min^{-1}. The rheological measurement was carried out on a stress controlled rheometer (rheometer System Gemini 200, Germany) using a 40 mm diameter parallel plate. During the rheological measurement process, the frequency sweep from 0.01 to 120 rad/s was performed at 200 °C under dry nitrogen atmosphere. For all the measurements, the samples were tested within the linear viscoelastic strain range.

The PECU/CNC−$C_6H_4NO_2$ (0, 5, 10, 20, and 30 wt %) films were cut into rectangular strips. The test specimen dimensions were 15 × 4

DOI: 10.1021/acsami.5b02940
ACS Appl. Mater. Interfaces 2015, 7, 12988−12999

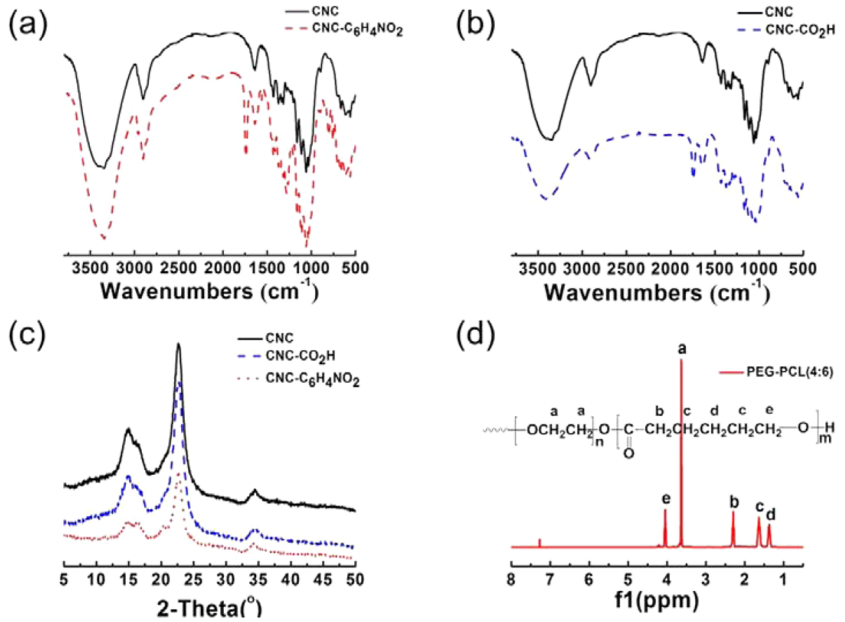

Figure 3. IR spectra of (a) CNC and CNC−$C_6H_4NO_2$ and (b) CNC−CO_2H; (c) XRD spectra of modified cellulose nanocrystals; and (d) ^1H NMR spectra of PCL−PEG-PCL (PEG/PCL = 4:6).

× 0.2 mm (length × width × thickness). The shape memory experimental description has already been provided.[38] The fixity ratio (R_f) was defined as θ_f/θ_i and the shape recovery ratio (R_r) was defined as $(\theta_f - \theta_r)/\theta_f$. The results represent the averages of at least three specimens. We also tested the shape memory effect of PECU/CNC−CO_2H (0, 5, 10, 20, and 30 wt %) films by immersing them in acidic and alkali solutions with different pH values. The shape recovery ratio and the fixity were repeated three times.

RESULTS AND DISCUSSION

Characterization of CNC−$C_6H_4NO_2$ and CNC−CO_2H. The morphological details of the cellulose nanocrystals and the modified cellulose nanocrystals (CNC−$C_6H_4NO_2$, CNC−CO_2H) were illustrated by TEM and DLS. As shown in Figure 2, the morphologies of CNCs, CNC−$C_6H_4NO_2$ and CNC−CO_2H are rod-like with length ranging from 200 to 300 nm and width of 5−20 nm. Figure 2d shows that the relative average particle size of the three nanofibers were 190, 210, and 240 nm accompanying with a uniform distribution. Thus, we could conclude that the modified conditions do not have further hydrolytic treatment on the CNCs, whose lengths were determined by the initial hydrolytic treatment. Therefore, the modification seemed to occur on the surface of CNCs.

FT-IR was employed to confirm the chemical structure of the CNC−$C_6H_4NO_2$ and CNC−CO_2H. From the spectra of the CNC−$C_6H_4NO_2$ in Figure 3a, we can find that CNCs show the characteristic peaks at 3343 (O−H), 2905 (C−H), 1640 (C═C), 1432 (−CH_2), and 1162 and 1056 (C−O−C) cm^{-1}. As a result of surface graft of pyridine moieties, the characteristic peaks of the aromatic rings of pyridine appeared at 1643 and 1600 (C═C) and 1535 (C═N) cm^{-1}.[49] The most important change was the appearance of 1730 (C═O) cm^{-1} stretching band, indicating that the hydroxyl group of CNCs reacted with pyridine-4-carbonyl chloride successfully.[48] Degree-of-substitution (DS) of CNC−$C_6H_4NO_2$ was 0.21, which calculated from the nitrogen content according to eq 1. Figure 3b confirms that the oxidized CNCs (CNC−CO_2H) was synthesized successfully, carboxyl content could be obtained from the area of the band at 1730 cm^{-1}. Meanwhile, only a slight reduction of the bands related to stretching vibration of O−H groups at 3343 cm^{-1} and C−H at 2905 cm^{-1} is observed.[52] The amount carboxyl groups and therefore the degree of oxidation (DO) of CNC−CO_2H could be detected by conductometric titrations. As shown in Figure S2 (Supporting Information), with the addition of sodium hydroxide, the carboxyl group on the modified CNCs was ionized, and then lead to change the conductivity.[52] According to conductometric titrations, we obtained the degree of oxidation is 0.18, which is less than the maximum theoretical DS 3 for modified cellulose under homogeneous conditions, indicating that not all of the surface hydroxyl groups are readily accessible, since some can be oriented toward the inner regime of the nanocrystals.[49] In Figure 3c, by comparison the diffraction peaks of nonmodified and modified cellulose nanocrystals, we can find that the cellulose I crystal structure is still reserved. Peaks appeared at 2θ 34.5, 22.5, 20.4, 17.6, and 15.8°, which belong to diffraction from (040), (002), (021), (110), and ($1\bar{1}0$) planes, respectively, of cellulose I. However, as a result of the modification, the peaks at 2θ 17.6 and 15.8° become a little different, which corresponded to (002) plane was broadened, indicating swelling of the nanocrystals in the reaction medium during chemical modification since the (002) plane consists of layered sheets of cellulose chains.[49] This is also evidence that the modification only occurs on the surface of CNCs as described before. The chemical structure of PCL−PEG-PCL polymer was investigated through ^1H NMR (Figure 3d). The disappearance of OH signal (4.7 ppm) from PEG indicates the reaction of OH groups with ε-CL. Whereas H-(a) at 3.65−3.69 ppm, H-(b) at 2.25−2.35 ppm, H-(c) at 1.59−1.71 ppm, H-(d) at 1.35−1.42 ppm, H-(e) at 4.05−4.1 ppm, all chemistry shift signals matched with the corresponding protons, indicate the successful synthesis of PCL−PEG-PCL.[53] From the intensity of signal H-(a) and H-(e), the repeating unit m was calculated and then M_n was deduced. Molecular weight of PCL−PEG-PCL is about 5.9 kDa measured by ^1H NMR, which is in agreement with the result (M_n 5.9, PDI 1.1) measured by GPC.

DOI: 10.1021/acsami.5b02940
ACS Appl. Mater. Interfaces 2015, 7, 12988−12999

X-ray photoelectron spectra (XPS) were used to determine the main elements and the carbon-based bonds of the CNC−$C_6H_4NO_2$. In Figure 4 low resolution spectra of all the

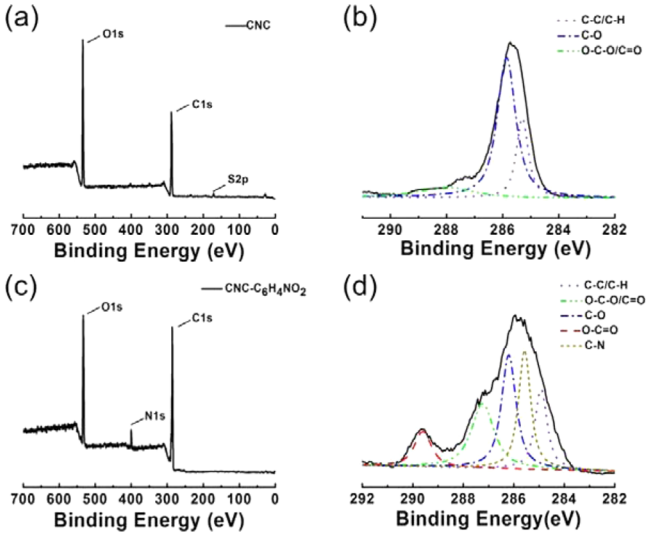

Figure 4. General XPS spectra for (a) CNC and (c) CNC−$C_6H_4NO_2$. Surface functional group composition as obtained from the XPS decomposition of the C 1s signal (b) CNC and (d) CNC−$C_6H_4NO_2$. High-resolution carbon spectra: C−C (C−H_x), 285.0 eV; C−O, 286.5 ± 0.1 eV; O−C−O/C═O, 288.05 ± 0.05 eV; O−C═O, 289.0 ± 0.1 eV; C−N, 286.2 eV.

nanocrystals show that carbon and oxygen atoms were the main components, while less nitrogen was indicates the presence of pyridine moieties. In the high-resolution carbon spectra, the carbon signal can be resolved into several component peaks, which reflect the local environments of the carbon atoms C−C(C−H_x), 285.0 eV; C−O, 286.5 ± 0.1 eV; O−C−O/C═O, 288.05 ± 0.05 eV; O−C═O, 289.0 ± 0.1 eV; and C−N, 286.2 eV.[54] The difference between CNC−$C_6H_4NO_2$ and CNCs was that the characteristic peaks of O−C═O and C−N appeared. These results also indicated that the hydroxyl groups of CNCs reacted with pyridine-4-carbonyl chloride successfully.

pH-Responsive Properties of the Modified Cellulose Nanocrystals. It is well-known that the pK_a value of pyridine is 5.19. At pH <5, pyridine accepts H^+, becoming protonated in acid.[38] The protonated N atom on the surface of CNC−$C_6H_4NO_2$ caused an increase in hydrophilia, it could be well distributed in the solution. When in base, H^+ was neutralized by OH^-, the N atom was deprotonated, CNC−$C_6H_4NO_2$ became hydrophobic and precipitates from aqueous solution because the interactions among the groups on the surface of CNC−$C_6H_4NO_2$ were formed.[42] As shown in Figure 5a,b, initially, both the CNCs and CNC−$C_6H_4NO_2$ appeared stable distributed in the solution at different pH values. After 30 min, however, the unmodified CNC suspensions remained insensitive to pH value, whereas above pH 5 the CNC−$C_6H_4NO_2$ were precipitated at the bottom of the bottle. The onset of flocculation was visible and continued over many hours. This transition was reversible; as the pH was shifted to values <5, a stable suspension was returned because the pyridyl groups were protonated again.[42] Figure 5c indicates that in an aqueous environment at high pH, the CNC−CO_2H were ionized and negatively charged, resulting in the electrostatic repulsions significantly reducing the attractive interactions between the CNC−CO_2H, and a homodisperse emulsion was obtained. Conversely, at low pH the CNC−CO_2H were deprotonated and in turn formed attractive interactions, which resulted from hydrogen bonding of the carboxylic acid and hydroxyl moieties, the onset of flocculation is visible. The pH-responsive function and surface zeta potential of CNC−$C_6H_4NO_2$ were quantified by DLS. As shown in Figure 5d, unmodified CNCs with sulfate ester groups were negatively

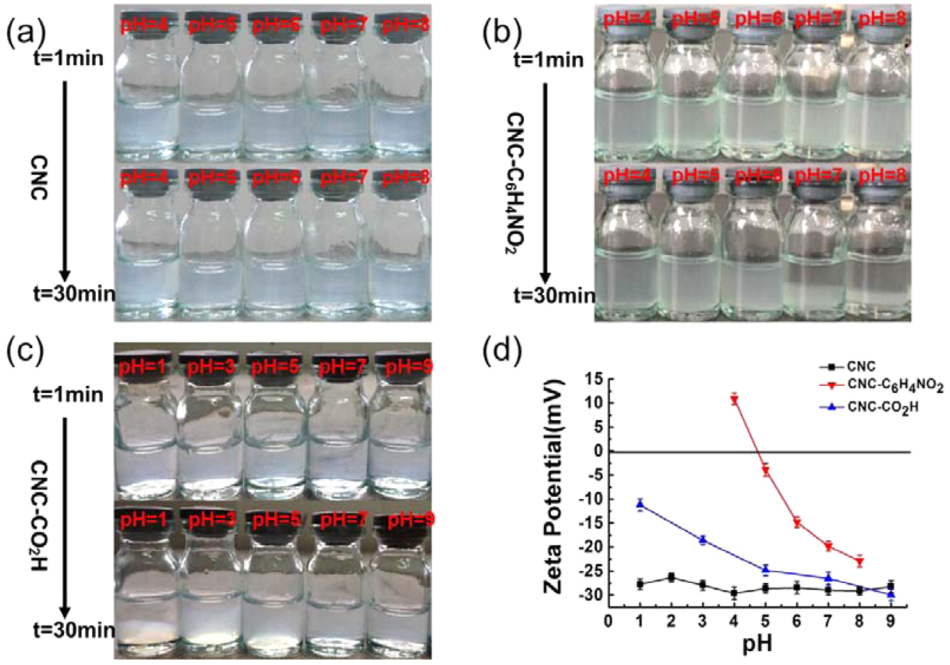

Figure 5. Photographs of (a) CNC, (b) CNC−$C_6H_4NO_2$, and (c) CNC−CO_2H suspensions (0.15 wt %) with different pH values for 1 and 30 min, respectively; (d) The zeta potential of modified cellulose nanocrystals placed in water solutions with different pH values. Experimental data represent average ± standard error.

DOI: 10.1021/acsami.5b02940
ACS Appl. Mater. Interfaces 2015, 7, 12988−12999

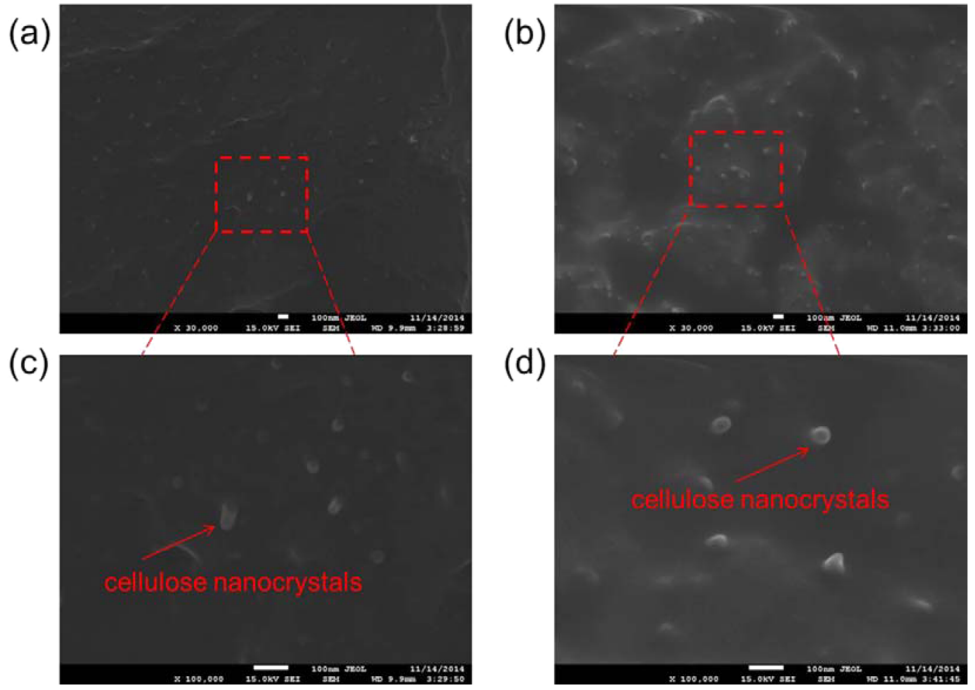

Figure 6. Cross-sectional SEM images showing the fracture surface of the PECU/CNCs nanocomposites: (a and c) PECU/CNC−$C_6H_4NO_2$ (10 wt %) and (b and d) PECU/CNC−$C_6H_4NO_2$ (20 wt %) magnified (a and b) 30 000× and (c and d) 100 000×. (Scale bar: 100 nm).

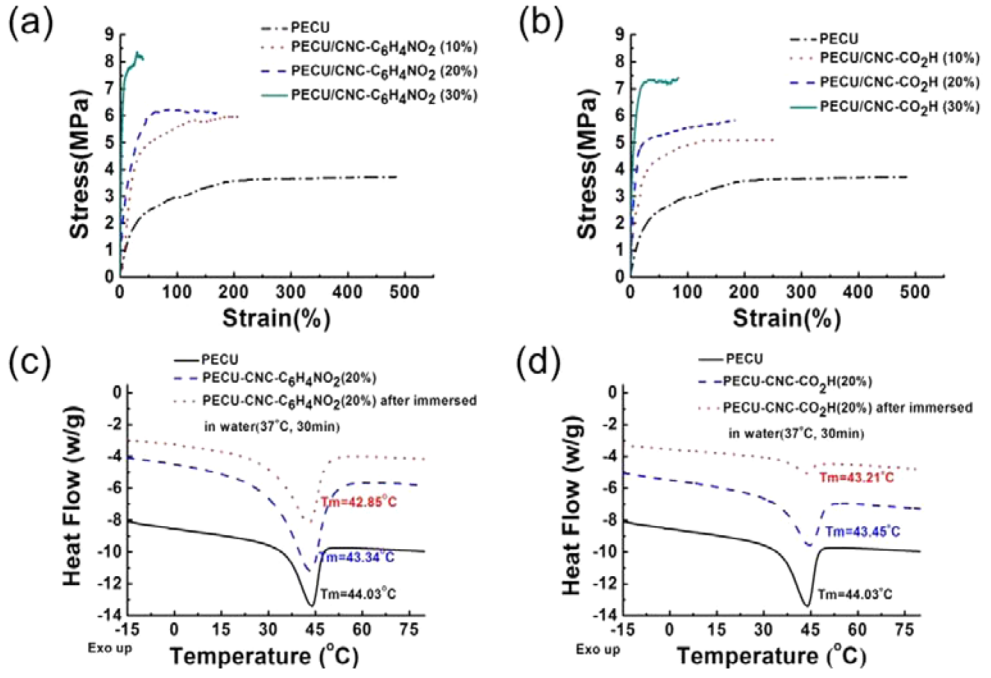

Figure 7. Typical stress−strain curves of the PECU/CNCs nanocomposite films with different CNCs loading: (a) PECU/CNC−$C_6H_4NO_2$ and (b) PECU/CNC−CO_2H. The DSC of PECU and its nanocomposites for (c) PECU/CNC−$C_6H_4NO_2$ (20 wt %) and (d) PECU/CNC−CO_2H (20 wt %).

charged due to sulfuric acid hydrolysis treatment. With the change of pH value of the solution, CNCs may be less changed. The value of zeta potential was relatively high, which could confirm that the solution is stable. The CNC−$C_6H_4NO_2$ had a positive electrophoretic mobility at pH values less than 5, which corresponds to a pyridyl groups protonated induced cationic surface charge. The value of zeta potential of the CNC−CO_2H was changed along with different value of pH. At pH < 7, the stability of the CNC−CO_2H solution was worse than that of CNCs, and the CNC−CO_2H solution appeared to be flocculating.

Morphology of the Nanocomposites. The fracture surface of samples, including PECU nanocomposites as a function of different CNC−$C_6H_4NO_2$ content, were observed by SEM. From Figure 6a,b, the white dots could be clearly identified in the matrix of the nanocomposites, which

DOI: 10.1021/acsami.5b02940
ACS Appl. Mater. Interfaces 2015, 7, 12988−12999

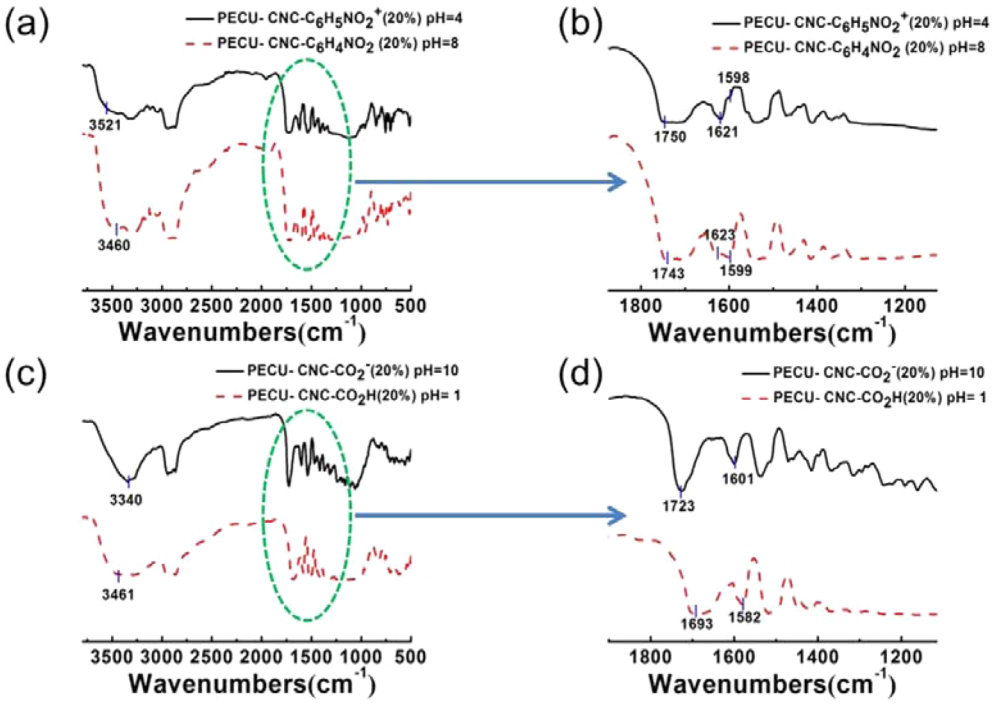

Figure 8. FT-IR spectra of (a and b) PECU/CNC−$C_6H_4NO_2$ (20 wt %) film after immersion in HCl solution (pH = 4) or NaOH solution (pH = 8) for 30 min; (c and d) PECU/CNC−CO_2H (20 wt %) film after immersion in HCl solution (pH = 1) and NaOH solution (pH = 10) for 30 min.

correspond to the CNC−$C_6H_4NO_2$ in the perpendicular plane of the nanocomposites.[55] Figure 6c,d, display the larger magnification of the fractured surface of the nanocomposite, and it could be obviously observed that the CNC−$C_6H_4NO_2$ fillers insert into the PECU matrix.[46] In addition, the solvent-exchange sol−gel process dispersed these CNC−$C_6H_4NO_2$ fillers in the PECU matrix; due to the hydrogen bonding between CNC−$C_6H_4NO_2$ and the molecular chains of the PECU, indicating that a good compatibility between the nanofillers and polymer matrix was achieved.[46] The CNC−$C_6H_4NO_2$ percolating network structure was formed in the nanocomposites due to the interactions among CNC−$C_6H_4NO_2$ as previously reported.[56]

Mechanical and Thermal Properties of the Nanocomposites. Figure 7a,b shows typical stress−strain curves for these nanocomposites, and the data, including elongation at break (ε_B), tensile strength (σ_B), and young's modulus (E), are summarized in Table S2 (Supporting Information). With the nanocrystals component increasing, the Young's modulus increased from 9.6 ± 0.3 to 54.2 ± 0.6 MPa; however, the elongation to break decreased 91%, which was attributed to a higher crystallinity and higher aspect ratio of the nanocrystals. In the nanocomposites, the enhancement in both strength and modulus is directly attributable to the reinforcement provided by cellulose nanofibrils dispersed at the nanoscale.[57,58] Additionally, with CNCs content increasing, the rigidity of the materials also increases, which is harmful to the shape memory recovery of polymer.[23]

Figure 7c,d shows the DSC results of the nanocomposites. The transition temperatures of all the nanocomposites were approximately 43 °C. Due to its better SME, the nanocomposite with modified CNCs of 20 wt % was selected to test. The transition temperature of the nanocomposite is slightly lower than that of pure PECU (44.5 °C), possibly due to an increase of the chain entanglement degree after the PECU mixed with nanocrystals. Moreover, after the nanocomposite is immersed in water at 37 °C for 30 min, the transition temperature cannot be changed. The reason may be that in this nanocomposite system, the polymer chains bond with modified CNCs via hydrogen bonds, and consequently, the water molecules have a very little influence on the movement of polymer chains. This is different from traditional ones, in which the water or other solvent dispersed in material matrix generally act as plasticizers to lower the glass transition temperature of shape memory polymers.[36]

Mechanism of the pH-Sensitivity. In acidic or alkali solutions, the primary condition to realize the pH-responsive SME based on hydrogen bonding interaction is that the material possesses good hydrophilicity, enabling H^+ or OH^- ions to diffuse into material matrix accompanying with H_2O molecules. The water contact angles of both PECU/CNC−$C_6H_4NO_2$ and PECU/CNC−CO_2H nanocomposites are approximately 75°; their swelling degrees get to more than 20% after immersion in acidic or alkali solutions for 90 min, indicating that they have good hydrophilicity (Figure S3, Supporting Information). In these nanocomposites, there are several kinds of H-bonding pairs, such as H-bonding interaction among COOH, NH, C═O, OH and electron-rich pyridine ring.[48] Figure 8 exhibits FT-IR spectra of PECU/CNC−$C_6H_4NO_2$ (20 wt %) film after immersion in HCl solution at pH = 4 or NaOH solution at pH = 8 for 30 min and PECU/CNC−CO_2H (20 wt %) film after immersion in HCl solution (pH = 1) or NaOH solution (pH = 10) for 30 min. There are significant differences between spectra in the acid and spectra in the base. The main contribution in the range of 3000−3500 cm^{-1} is due to O−H stretching, whereas the 1500−1750 cm^{-1} region is attributed to the NH, C═O and pyridine ring. The main peaks are located at 1500−1750 cm^{-1} and 3000−3500 cm^{-1} regions because the hydrogen bond of the materials caused wavenumbers to shift lower and wider. In the acid, the

DOI: 10.1021/acsami.5b02940
ACS Appl. Mater. Interfaces 2015, 7, 12988−12999

pyridine on the surface of CNC−$C_6H_4NO_2$ was protonated, leading to the damage of H-bonding interactions of isocyanate groups of PECU and pyridine of CNC−$C_6H_4NO_2$. The vibration peak of the pyridine ring at 1598 cm^{-1} disappeared in acid, indicating that the hydrogen bond between N−H and the pyridine ring was destroyed by protonation of pyridine in acid.[38] In the base, the pyridine on the surface of CNC−$C_6H_4NO_2$ was deprotonated, causing the formation of the H-bonding interactions among nanocrystals and materials. H-bonding interactions between the carboxyl groups on the surface of CNC−CO_2H and isocyanate groups of PECU were also confirmed by FT-IR. CNC−CO_2H responded to pH variation in an opposite manner with CNC−$C_6H_4NO_2$ (Figure 1 and Figure S1, Supporting Information).

Figure 9 gives the dependence of storage modulus G' on frequency for pure PECU and its nanocomposites. With

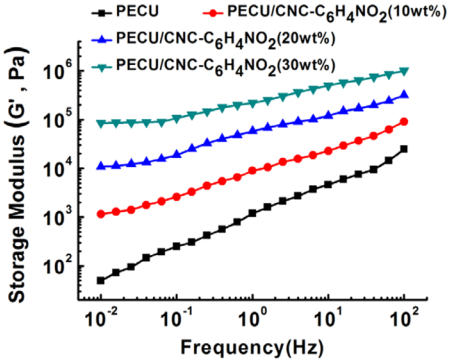

Figure 9. Rheological properties of PECU/CNC−$C_6H_4NO_2$ nanocomposite with different CNCs loading about storage modulus (G') as a function of frequency.

modified cellulose nanocrystal content increasing, G' of the nanocomposites were significantly enhanced and became less dependent on frequency throughout the test range.[59] The diminished dependence on frequency indicates that the formation of modified cellulose nanocrystals networks. The percolated networks of filler are often quantified by a plateau in the dynamic moduli at low frequencies.[59] In this system, the nanocomposite exhibits pH-sensitivity SME through the association and dissociation of the hydrogen bonding interactions between the modified CNC percolation network and matrix materials, which would be formed and destroyed via changing pH values. The pH-sensitive modified CNCs percolation network in matrix materials served as the switch units of SMPs.

pH-Responsive Shape-Memory Properties of the Nanocomposites. The effect of pH value of both acidic or alkali solutions on the shape memory function was first optimized. From Figure S4 (Supporting Information), it can be seen that for PECU/CNC−$C_6H_4NO_2$ nanocomposite, at pH = 4 it was easily protonated, leading to the disassociation of hydrogen bonding interactions and subsequently acquiring the shape recovery with the highest recovery ratio; at pH = 8 it was also readily deprotonated, causing the association of hydrogen bonding interactions and in turn achieving the shape fixity with the highest fixity ratio. Therefore, the pH values of 4 and 8 are chosen to investigate the pH-responsive shape memory of PECU/CNC−$C_6H_4NO_2$ nanocomposite. Similarly, the pH values of 1 and 10 are optimized for PECU/CNC−CO_2H nanocomposite. The digital photos in Figure 10a display the shape memory process of PECU/CNC−$C_6H_4NO_2$ nanocomposites with CNC−$C_6H_4NO_2$ concentrations from 0 to 30 wt % immersed in HCl solution (pH = 4) and NaOH solution (pH = 8). First, a straight strip was immersed in HCl solution for 30 min to destroy hydrogen bonding interactions; and then the strip was folded by constant stress conditions to fix the temporary shape in NaOH solution. After 5 min, the force was removed, and the temporary shape was maintained. After that, the deformed sample was immersed in HCl solution for 30 min and gradually recovered to a strip again. Among these materials, the nanocomposite with 20 wt % CNC−$C_6H_4NO_2$ performed the most excellent shape memory properties with both R_f and R_r more than 85% (Figure 10b). The temporary shape of the nanocomposites could be fixed, however, the pure PECU materials could not fix at the same condition, which proved that the pH-sensitive modified CNCs percolation network in matrix materials served as the switch units of SMPs to fix the temporary shape. With the content of CNC−$C_6H_4NO_2$ increasing, the hydrogen bonding interactions became stronger and the switch units of SMPs were more complete, leading to an increase of R_f. However, with the content of CNC−$C_6H_4NO_2$ increasing, the R_r slightly reduced. This phenomenon may be influenced by the variation of mechanical properties with the introduced of nanocrystals.[23] The shape memory effect of PECU/CNC−CO_2H was similar to PECU/CNC−$C_6H_4NO_2$ nanocomposite, but the pH value for triggering SME is opposite to it (Figure S5, Supporting Information).

The influence of cycle times of shape memory test on shape memory properties was further investigated. As shown in Figure 10c, with the cycle time of shape memory test increasing, the R_f remained more than 80% because the percolation network and hydrogen bonding interactions were not destroyed. However, the R_r decreased from 82 to 65% after six cyclic shape memory tests. In general, the values of R_f and R_r for each sample are relatively stable, showing good repeatability, despite the R_r decreases with increasing cycle number, presumably due to the orientation of modified CNCs along the stretch direction.[60]

CONCLUSIONS

In summary, we have successfully developed one type of novel pH-responsive shape-memory polymer nanocomposite with modified CNC percolation networks. The introduction of PCL−PEG-PCL can improve biodegradability and biocompatibility of PU. CNCs functionalized with carboxyl groups (CNC−CO_2H) and pyridine moieties (CNC−$C_6H_4NO_2$) endow the pH-responsiveness of CNCs via the association and disassociation of hydrogen bonding interactions among CNCs under different pH conditions. In the polymer nanocomposite, the pH-sensitive CNCs percolation network between CNCs and CNCs with polymer chains not only improved the mechanical properties obviously but also served as switch units of shape memory function. The excellent pH-sensitive shape memory effect can be readily controlled through changing hydrogen bonding interaction via altering the pH of the environment. The pH-responsive shape memory polymer nanocomposite can be potentially applied as biomaterials, smart actuators, and sensors.

DOI: 10.1021/acsami.5b02940
ACS Appl. Mater. Interfaces 2015, 7, 12988−12999

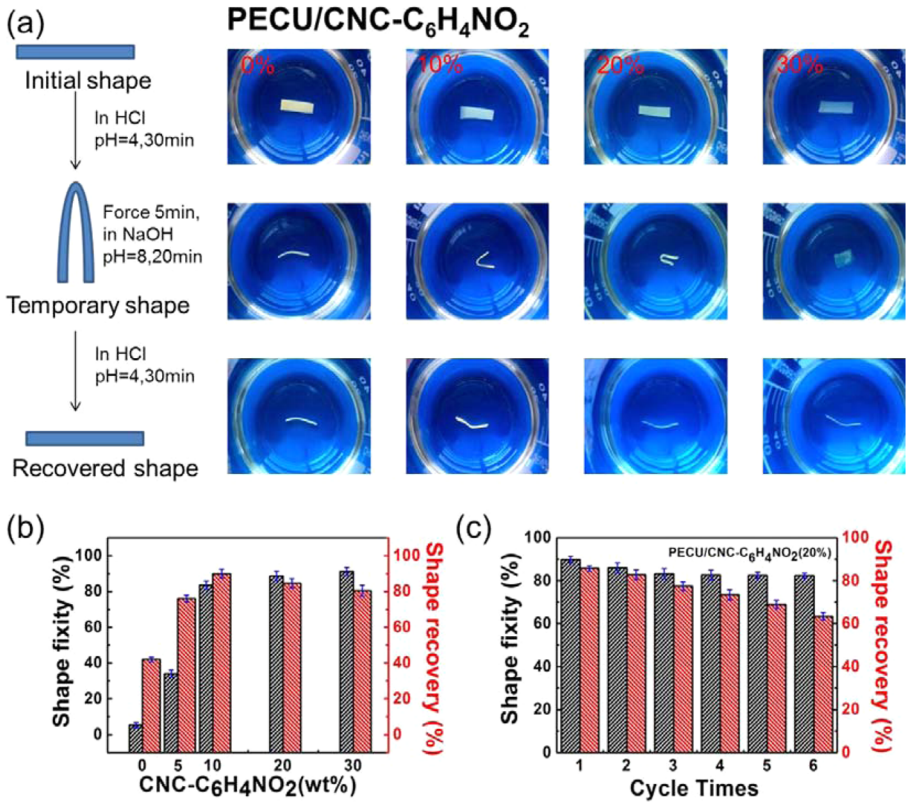

Figure 10. (a) Digital photos showing the shape memory process of PECU/CNC−$C_6H_4NO_2$ film (15 × 4 × 0.2 mm) with different CNC−$C_6H_4NO_2$ loading immersed in HCl solution (pH = 4) and NaOH solution (pH = 8) at room temperature. (b) Shape memory properties of PECU and its nanocomposites as a function of CNC−$C_6H_4NO_2$ content. (c) Shape memory properties of PECU/CNC−$C_6H_4NO_2$ (20 wt %) versus cycle times. Experimental data represent average ± standard error.

■ ASSOCIATED CONTENT

Supporting Information

Shape memory function, water contact angle, mechanical properties of PECU/CNC-$C_6H_4NO_2$ nanocomposites. The Supporting Information is available free of charge on the ACS Publications website at DOI: 10.1021/acsami.5b02940.

■ AUTHOR INFORMATION

Corresponding Author

*Tel: +86 28 87634068. Fax: +86 28 87634649. E-mail: shaobingzhou@swjtu.edu.cn.

Notes

The authors declare no competing financial interest.

■ ACKNOWLEDGMENTS

This work was partially supported by the National Basic Research Program of China (973 Program, 2012CB933600), the National Natural Science Foundation of China (51173150, 51373138), the National Key Project of Scientific and Technical Supporting Programs Funded by MSTC (2012BAI17B06), the Research Fund for the Doctoral Program of Higher Education of China (20120184110029), and the Construction Program for Innovative Research Team of University in Sichuan Province (14TD0050).

■ REFERENCES

(1) Behl, M.; Razzaq, M. Y.; Lendlein, A. Multifunctional Shape-Memory Polymers. *Adv. Mater.* **2010**, *22*, 3388−3410.

(2) Garle, A.; Kong, S.; Ojha, U.; Budhlall, B. M. Thermoresponsive Semicrystalline Poly(ε-caprolactone) Networks: Exploiting Cross-Linking with Cinnamoyl Moieties to Design Polymers with Tunable Shape Memory. *ACS Appl. Mater. Interfaces* **2012**, *4*, 645−657.

(3) Miaudet, P.; Derré, A.; Maugey, M.; Zakri, C.; Piccione, P. M.; Inoubli, R.; Poulin, P. Shape and Temperature Memory of Nanocomposites with Broadened Glass Transition. *Science* **2007**, *318*, 1294−1296.

(4) Zheng, X. T.; Zhou, S. B.; Li, X. H.; Weng, J. Shape Memory Properties of Poly(D,L-lactide)/Hydroxyapatite Composites. *Biomaterials* **2006**, *27*, 4288−4295.

(5) Lendlein, A.; Jiang, H.; Jünger, O.; Langer, R. Light-Induced Shape-Memory Polymers. *Nature* **2005**, *434*, 879−882.

(6) Jiang, H.; Kelch, S.; Lendlein, A. Polymers Move in Response to Light. *Adv. Mater.* **2006**, *18*, 1471−1475.

(7) Liu, Y.; Lv, H.; Lan, X.; Leng, J.; Du, S. Review of Electro-Active Shape-Memory Polymer Composite. *Compos. Sci. Technol.* **2009**, *69*, 2064−2068.

(8) Luo, X.; Mather, P. T. Conductive Shape Memory Nanocomposites for High Speed Electrical Actuation. *Soft Matter* **2010**, *6*, 2146−2149.

(9) Xiao, Y.; Zhou, S. B.; Wang, L.; Gong, T. Electro-Active Shape Memory Properties of Poly(epsilon-caprolactone)/Functionalized Multiwalled Carbon Nanotube Nanocomposite. *ACS Appl. Mater. Interfaces* **2010**, *2*, 3506−3514.

(10) Mohr, R.; Kratz, K.; Weigel, T.; Lucka-Gabor, M.; Moneke, M.; Lendlein, A. Initiation of Shape-Memory Effect by Inductive Heating of Magnetic Nanoparticles in Thermoplastic Polymers. *P. Natl. Acad. Sci. USA* **2006**, *103*, 3540−3545.

(11) Zheng, X. T.; Zhou, S. B.; Xiao, Y.; Yu, X. J.; Li, X. H.; Wu, P. Z. Shape Memory Effect of Poly(D,L-lactide)/Fe_3O_4 Nanocomposites by Inductive Heating of Magnetite Particles. *Colloid. Surface. B* **2009**, *71*, 67−72.

DOI: 10.1021/acsami.5b02940
ACS Appl. Mater. Interfaces 2015, 7, 12988−12999

(12) Du, H.; Zhang, J. Solvent Induced Shape Recovery of Shape Memory Polymer Based on Chemically Cross-Linked Poly(vinyl alcohol). *Soft Matter* **2010**, *6*, 3370−3376.
(13) Lv, H.; Leng, J.; Liu, Y.; Du, S. Shape-Memory Polymer in Response to Solution. *Adv. Eng. Mater.* **2008**, *10*, 592−595.
(14) Chen, S.; Hu, J.; Zhuo, H. Study on the Moisture Absorption of Pyridine Containing Polyurethane for Moisture-Responsive Shape Memory Effects. *J. Mater. Sci.* **2011**, *46*, 6581−6588.
(15) Aoki, D.; Teramoto, Y.; Nishio, Y. SH-Containing Cellulose Acetate Derivatives: Preparation and Characterization as a Shape Memory Recovery Material. *Biomacromolecules* **2007**, *8*, 3749−3757.
(16) Liu, L.; Wang, N.; Han, Y.; Li, Y.; Liu, W. Redox-Triggered Self-Rolling Robust Hydrogel Tubes for Cell Encapsulation. *Macromol. Rapid Commun.* **2014**, *35*, 344−349.
(17) Serrano, M.; Ameer, G. Recent Insights Into the Biomedical Applications of Shape-Memory Polymers. *Macromol. Biosci.* **2012**, *12*, 1156−1171.
(18) Rodriguez, J.; Yu, Y.; Miller, M.; Wilson, T.; Hartman, J.; Clubb, F.; Gentry, B.; Maitland, D. Opacification of Shape Memory Polymer Foam Designed for Treatment of Intracranial Aneurysms. *Ann. Biomed. Eng.* **2012**, *40*, 883−897.
(19) Yu, X. J.; Wang, L.; Huang, M. T.; Gong, T.; Li, W. B.; Cao, Y. L.; Ji, D. J.; Wang, P.; Wang, J.; Zhou, S. B. A Shape Memory Stent of Poly(ε-caprolactone-co-DL-lactide) Copolymer for Potential Treatment of Esophageal Stenosis. *J. Mater. Sci.: Mater. Med.* **2012**, *23*, 581−589.
(20) Liu, X.; Zhao, K.; Gong, T.; Song, J.; Bao, C. Y.; Luo, E.; Weng, J.; Zhou, S. B. Delivery of Growth Factors Using a Smart Porous Nanocomposite Scaffold to Repair a Mandibular Bone Defect. *Biomacromolecules* **2014**, *15*, 1019−1030.
(21) Wischke, C.; Neffe, A. T.; Steuer, S.; Lendlein, A. Evaluation of a Degradable Shape-Memory Polymer Network as Matrix for Controlled Drug Release. *J. Controlled Release* **2009**, *138*, 243−250.
(22) Gong, T.; Zhao, K.; Wang, W. X.; Chen, H. M.; Wang, L.; Zhou, S. B. Thermally Activated Reversible Shape Switch of Polymer Particles. *J. Mater. Chem. B* **2014**, *2*, 6855−6866.
(23) Madbouly, S.; Lendlein, A. Shape-Memory Polymer Composites. *Adv. Polym. Sci.* **2010**, *226*, 41−95.
(24) Zhang, Y.; Wang, Q.; Wang, C.; Wang, T. High-Strain Shape Memory Polymer Networks Crosslinked by SiO_2. *J. Mater. Chem.* **2011**, *21*, 9073−9078.
(25) Gunes, I. S.; Cao, F.; Jana, S. C. Evaluation of Nanoparticulate Fillers for Development of Shape Memory Polyurethane Nanocomposites. *Polymer* **2008**, *49*, 2223−2234.
(26) Sahoo, N. G.; Jung, Y. C.; Yoo, H. J.; Cho, J. W. Influence of Carbon Nanotubes and Polypyrrole on the Thermal, Mechanical and Electroactive Shape-Memory Properties of Polyurethane Nanocomposites. *Compos. Sci. Technol.* **2007**, *67*, 1920−1929.
(27) Li, W. B.; Gong, T.; Chen, H. M.; Wang, L.; Li, J. R.; Zhou, S. B. Tuning Surface Micropattern Features Using a Shape Memory Functional Polymer. *RSC Adv.* **2013**, *3*, 9865−9874.
(28) Habibi, Y.; Lucia, L. A.; Rojas, O. J. Cellulose Nanocrystals: Chemistry, Self-Assembly, and Applications. *Chem. Rev.* **2010**, *110*, 3479−3500.
(29) Azizi Samir, M. A. S.; Alloin, F.; Dufresne, A. Review of Recent Research into Cellulosic Whiskers, their Properties and their Application in Nanocomposite Field. *Biomacromolecules* **2005**, *6*, 612−626.
(30) Leng, J.; Lan, X.; Liu, Y.; Du, S. Shape-Memory Polymers and their Composites: Stimulus Methods and Applications. *Prog. Mater. Sci.* **2011**, *56*, 1077−1135.
(31) Meng, H.; Li, G. Q. A Review of Stimuli-Responsive Shape Memory Polymer Composites. *Polymer* **2013**, *54*, 2199−2221.
(32) Erb, R. M.; Sander, J. S.; Grisch, R.; Studart, A. R. Self-Shaping Composites with Programmable Bioinspired Microstructures. *Nat. Commun.* **2013**, *4*, 1712−1719.
(33) Mendez, J.; Annamalai, P. K.; Eichhorn, S. J.; Rusli, R.; Rowan, S. J.; Foster, E. J.; Weder, C. Bioinspired Mechanically Adaptive Polymer Nanocomposites with Water-Activated Shape-Memory Effect. *Macromolecules* **2011**, *44*, 6827−6835.
(34) Zhu, Y.; Hu, J. L.; Luo, H.; Young, R. J.; Deng, L. B.; Zhang, S.; Fan, Y.; Ye, G. D. Rapidly Switchable Water-Sensitive Shape-Memory Cellulose/Elastomer Nano-Composites. *Soft Matter* **2012**, *8*, 2509−2517.
(35) Capadona, J. R.; Shanmuganathan, K.; Tyler, D. J.; Rowan, S. J.; Weder, C. Stimuli-Responsive Polymer Nanocomposites Inspired by the Sea Cucumber Dermis. *Science* **2008**, *319*, 1370−1374.
(36) Liu, Y.; Li, Y.; Chen, H. M.; Yang, G.; Zheng, X. T.; Zhou, S. B. Water-Induced Shape-Memory Poly(D,L-lactide)/Microcrystalline Cellulose Composites. *Carbohydr. Polym.* **2014**, *104*, 101−108.
(37) Fleige, E.; Quadir, M. A.; Haag, R. Stimuli-Responsive Polymeric Nanocarriers for the Controlled Transport of Active Compounds: Concepts and Applications. *Adv. Drug Deliver. Rev.* **2012**, *64*, 866−884.
(38) Chen, H. M.; Li, Y.; Liu, Y.; Gong, T.; Wang, L.; Zhou, S. B. Highly pH-Sensitive Polyurethane Exhibiting Shape Memory and Drug Release. *Polym. Chem.* **2014**, *5*, 5168−5174.
(39) Han, X. J.; Dong, Z. Q.; Fan, M. M.; Liu, Y.; Li, J. H.; Wang, Y. F.; Yuan, Q. J.; Li, B. J.; Zhang, S. pH-Induced Shape-Memory Polymers. *Macromol. Rapid Commun.* **2012**, *33*, 1055−1060.
(40) Guo, W.; Lu, C. H.; Orbach, R.; Wang, F.; Qi, X. J.; Cecconello, A.; Seliktar, D.; Willner, I. pH-Stimulated DNA Hydrogels Exhibiting Shape-Memory Properties. *Adv. Mater.* **2015**, *27*, 73−78.
(41) Wu, T.; Su, Y.; Chen, B. Mechanically Adaptive and Shape-Memory Behaviour of Chitosan-Modified Cellulose Whisker/Elastomer Composites in Different pH Environments. *ChemPhysChem* **2014**, *15*, 2794−2800.
(42) Kan, K.; Li, J.; Wijesekera, K.; Cranston, E. Polymer-Grafted Cellulose Nanocrystals as pH-Responsive Reversible Flocculants. *Biomacromolecules* **2013**, *14*, 3130−3139.
(43) Way, A.; Hsu, L.; Shanmuganathan, K.; Weder, C.; Rowan, S. pH-Responsive Cellulose Nanocrystal Gels and Nanocomposites. *ACS Macro Lett.* **2012**, *1*, 1001−1006.
(44) Hu, J. L.; Zhu, Y.; Huang, H. H.; Lu, J. Recent Advances in Shape−Memory Polymers: Structure, Mechanism, Functionality, Modeling, and Applications. *Prog. Polym. Sci.* **2012**, *37*, 1720−1763.
(45) Bondeson, D.; Mathew, A.; Oksman, K. Optimization of the Isolation of Nanocrystals from Microcrystalline Cellulose by Acid Hydrolysis. *Cellulose* **2006**, *13*, 171−180.
(46) Liu, Y.; Li, Y.; Yang, G.; Zheng, X. T.; Zhou, S. B. Multi-Stimulus-Responsive Shape-Memory Polymer Nanocomposite Network Cross-Linked by Cellulose Nanocrystals. *ACS Appl. Mater. Interfaces* **2015**, *7*, 4118−4126.
(47) Saralegi, A.; Gonzalez, M.; Valea, A.; Eceiza, A.; Corcuera, M. The Role of Cellulose Nanocrystals in the Improvement of the Shape-Memory Properties of Castor Oil-Based Segmented Thermoplastic Polyurethanes. *Compos. Sci. Technol.* **2014**, *92*, 27−33.
(48) Chen, H. M.; Liu, Y.; Gong, T.; Wang, L.; Zhao, K. Q.; Zhou, S. B. Use of Intermolecular Hydrogen Bonding to Synthesize Triple-Shape Memory Supermolecular Composites. *RSC Adv.* **2013**, *3*, 7048−7056.
(49) Hassana, M.; Moorefieldb, C.; Elbatal, H.; Newkomeb, G.; Modarellid, D.; Romano, N. Fluorescent Cellulose Nanocrystals via Supramolecular Assembly of Terpyridine-Modified Cellulose Nanocrystals and Terpyridine-Modified Perylene. *Mater. Sci. Eng., B* **2012**, *177*, 350−358.
(50) Habibi, Y.; Chanzy, H.; Vignon, M. TEMPO-Mediated Surface Oxidation of Cellulose Whiskers. *Cellulose* **2006**, *13*, 679−687.
(51) Zhou, S. B.; Deng, X. M.; Yang, H. Biodegradable Poly(ε-Caprolactone)−Poly(Ethylene Glycol) Block Copolymers: Characterization and Their Use as Drug Carriers for a Controlled Delivery System. *Biomaterials* **2003**, *24*, 3563−3570.
(52) Perez, D.; Montanari, S.; Vignon, M. TEMPO-Mediated Oxidation of Cellulose III. *Biomacromolecules* **2003**, *4*, 1417−1425.
(53) Yang, X. F.; Wang, L.; Wang, W. X.; Chen, H. M.; Yang, G.; Zhou, S. B. Triple Shape Memory Effect of Star-Shaped Polyurethane. *ACS Appl. Mater. Interfaces* **2014**, *6*, 6545−6554.

DOI: 10.1021/acsami.5b02940
ACS Appl. Mater. Interfaces 2015, 7, 12988−12999

(54) Lin, N.; Dufresne, A. Physical and/or Chemical Compatibilization of Extruded Cellulose Nanocrystal Reinforced Polystyrene Nanocomposites. *Macromolecules* **2013**, *46*, 5570−5583.
(55) Zhao, Q.; Sun, G.; Yan, K.; Zhou, A.; Chen, Y. Novel Bio-Antifelting Agent Based on Waterborne Polyurethane and Cellulose Nanocrystals. *Carbohydr. Polym.* **2013**, *91*, 169−174.
(56) Annamalai, P.; Dagnon, K.; Monemian, S.; Foster, E.; Rowan, S.; Weder, C. Water-Responsive Mechanically Adaptive Nanocomposites Based on Styrene−Butadiene Rubber and Cellulose Nanocrystals Processing Matters. *ACS Appl. Mater. Interfaces* **2014**, *6*, 967−976.
(57) Marcovich, N.; Auad, M.; Bellesi, N.; Nutt, S.; Aranguren, M. Cellulose Micro/Nanocrystals Reinforced Polyurethane. *J. Mater. Res.* **2006**, *21*, 870−881.
(58) Wu, Q.; Henriksson, M.; Liu, X.; Berglund, L. A High Strength Nanocomposite Based on Microcrystalline Cellulose and Polyurethane. *Biomacromolecules* **2007**, *8*, 3687−3692.
(59) Gao, C.; Zhang, S.; Wang, F.; Wen, B.; Han, C.; Ding, Y.; Yang, M. Graphene Networks with Low Percolation Threshold in ABS Nanocomposites: Selective Localization and Electrical and Rheological Properties. *ACS Appl. Mater. Interfaces* **2014**, *6*, 12252−12260.
(60) Wu, T.; Kelly, K.; Chen, B. Poly(methacrylic acid)-Grafted Clay−Thermoplastic Elastomer Composites with Water-Induced Shape-Memory Effects. *J. Polym. Sci., Part B: Polym. Phys.* **2013**, *51*, 1513−1522.

DOI: 10.1021/acsami.5b02940
ACS Appl. Mater. Interfaces 2015, 7, 12988−12999